Trametes versicolor glutathione transferase Xi 3, a dual Cys-GST with catalytic specificities of both Xi and Omega classes

Mathieu Schwartz, Thomas Perrot, Aurélie Deroy, Thomas Roret, Melanie Morel-Rouhier, Guillermo Mulliert, Eric Gelhaye, Frédérique Favier, Claude Didierjean

FEBS Letters

FEBS PRESS science publishing by scientists

Trametes versicolor glutathione transferase Xi 3, a dual Cys-GST with catalytic specificities of both Xi and Omega classes

Mathieu Schwartz[1], Thomas Perrot[2], Aurélie Deroy[2], Thomas Roret[3], Mélanie Morel-Rouhier[2], Guillermo Mulliert[1], Eric Gelhaye[2], Frédérique Favier[1] and Claude Didierjean[1]

1 CNRS, CRM2, Université de Lorraine, Nancy, France
2 INRA, IAM, Université de Lorraine, Nancy, France
3 CNRS, LBI2M, Sorbonne Université, Roscoff, France

Correspondence
C. Didierjean, CNRS, CRM2, Université de Lorraine, Nancy 54506, France
Fax: +33 383684300
Tel: +33 372745642
E-mail: Claude.didierjean@univ-lorraine.fr

Mathieu Schwartz and Thomas Perrot contributed equally to this work.

(Received 18 May 2018, revised 9 August 2018, accepted 11 August 2018, available online 6 September 2018)

doi:10.1002/1873-3468.13224

Edited by Stuart Ferguson

Glutathione transferases (GSTs) from the Xi and Omega classes have a catalytic cysteine residue, which gives them reductase activities. Until now, they have been assigned distinct substrates. While Xi GSTs specifically reduce glutathionyl-(hydro)quinones, Omega GSTs are specialized in the reduction of glutathionyl-acetophenones. Here, we present the biochemical and structural analysis of TvGSTX1 and TvGSTX3 isoforms from the wood-degrading fungus *Trametes versicolor*. TvGSTX1 reduces GS-menadione as expected, while TvGSTX3 reduces both Xi and Omega substrates. An in-depth structural analysis indicates a broader active site for TvGSTX3 due to specific differences in the nature of the residues situated in the C-terminal helix α9. This feature could explain the catalytic duality of TvGSTX3. Based on phylogenetic analysis, we propose that this duality might exist in saprophytic fungi and ascomycetes.

Keywords: crystallography; dual enzyme activity; glutathione transferase Xi; glutathionyl-acetophenone reductase; glutathionyl-hydroquinone reductase

Glutathione transferases (GSTs) are widespread enzymes, which use glutathione (GSH) through several different types of reactions. Most GSTs that harbor a catalytic serine residue (Ser-GSTs) or a catalytic tyrosine residue (Tyr-GSTs) exhibit glutathione-transferase activity, and GSTs with a catalytic cysteine residue (Cys-GSTs) mainly possess glutathione-lyase activity (i.e. deglutathionylation) [1]. Cys-GSTs biochemically characterized so far are subdivided into at least six classes, Beta [2], CLIC [3], dehydroascorbate reductases [4], Omega [5], Lambda [6,7], and Xi [8]. GSTs adopt a conserved fold composed of two domains, namely an N-terminal thioredoxin-like domain, and a C-terminal α-helical domain. The active site, located in a cleft at the interface between domains, consists of a GSH-binding site (G site) and a hydrophobic moiety-binding site (H site). While Ser-GSTs and Tyr-GSTs are mainly dimeric, Cys-GSTs show more structural diversity. Indeed, GSTLs, DHARs, and CLICs are monomeric, GSTBs and GSTOs assemble through the canonical dimer, and Xi class GSTs (GSTXs) form an atypical dimer.

Omega class GST (GSTO) isoforms from human (HsGSTO1) and from the white rot fungus

Abbreviations
CDNB, 1-chloro 2,4-dinitrobenzene; ESRF, European synchrotron radiation facility; GHR, glutathionyl-hydroquinone reductase; GSH, glutathione; GS-MEN, glutathionyl-menadione; GS-PAP, glutathionyl-phenylacetophenone; GST, glutathione transferase; GSTO, Omega class GST; GSTX, Xi class GST; JGI, joint genome institute; PDB, protein data bank; rmsd, root mean square deviation.

Phanerochaete chrysosporium (PcGSTO3 and PcGSTO4) have been shown to catalyze specific reduction of glutathionyl-acetophenones [8–10] (Fig. 1). Board and coworkers proposed a reaction mechanism for human isoform HsGSTO1[9]. The catalytic thiolate is assumed to attack the thioether sulfur atom to give an acetophenone enolate and a mixed disulfide between GSH and C32 of HsGSTO1. The enolate is readily protonated to produce the acetophenone. Then a molecule of GSH reduces the active site disulfide bond and achieves enzyme regeneration. The crystal structure of an enzyme–substrate complex provided no insight into the reaction mechanism. Indeed, the structure of the mutant HsGSTO1^{C32A} in complex with glutathionyl-nitroacetophenone (GS-NAP) revealed the substrate bound in a site too far from the active site to be of catalytic relevance [11].

GSTs of the Xi class constitute a distinct phylogenetic group [12] that has been characterized through multiple studies in bacteria (PcpF from *Sphingobium chlorophenolicum* [13] and YqjG from *Escherichia coli* [14]), fungi (ECM4 from *Saccharomyces cerevisiae* [15,16], PcGSTX1 from *P. chrysosporium* previously named PcGHR1 [8]), and plants (PtGHR1 and PtGHR2 from poplar [17]). Contrary to GSTOs, GSTXs do not reduce glutathionyl-acetophenones but exhibit specific activity in reducing glutathionyl-(hydro)quinones [18,19] (Fig. 1). GSTXs have been initially named glutathionyl-hydroquinone reductases (GHRs) and such activity was not detected for GSTO isoforms [18,20]. Green and coworkers [14] proposed that three tyrosine residues and a cysteine within the active site contribute to the catalytic activity of Xi GSTs. First, the attack of the substrate by the catalytic thiolate together with an acid catalysis by the tyrosine cluster result in a mixed disulfide bond Cys-S-SG and a protonated hydroquinone.

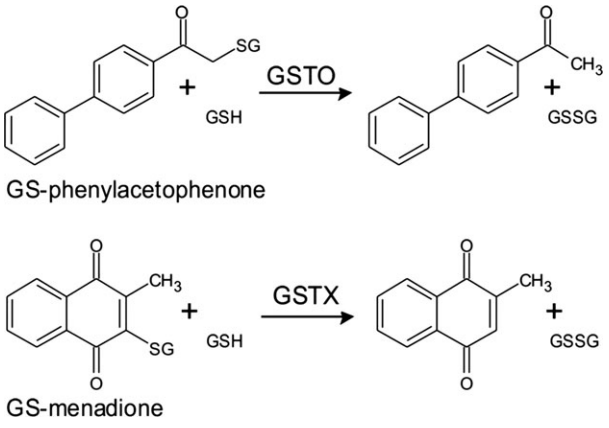

Fig. 1. Reactions catalyzed by GSTOs and GSTXs.

Then, the tyrosine triad acts as a base to activate a second GSH molecule during the regenerative process. Structural comparisons based on the crystal structure of *E. coli* YqjG isoform in complex with glutathionyl-menadione (GS-MEN) enabled a description of the residues involved in the hydroquinone stabilization [15,21]. The putative roles of five residues, F228, Y224, H345, H350, and W48 (ECM4 numbering) emerged from the active site analysis. The tyrosine and phenylalanine residues could stabilize the aromatic moiety of the substrate. The nitrogen atom of the W48 indole group and a water molecule coordinated by both histidine residues could interact with the carbonyl–quinone groups.

In this study, we present the biochemical and structural analysis of the GST isoforms X1 and X3 from the white rot *T. versicolor*. While both possess a GHR function as expected, TvGSTX3 has a surprising additional activity so far thought to be specific to GSTOs [9]. A crystallographic study helped in determining the molecular features that could explain this original profile. Then, a phylogenetic analysis focused on fungal GSTXs investigated the possible distribution of this catalytic diversity.

Materials and methods

Cloning, mutagenesis, expression, and purification

Synthetic genes encoding TvGSTX1 [Joint Genome Institute (JGI) accession number: Tv66368], TvGSTX3 (Tv73942), mutant TvGSTX3^{S295H} were purchased from GeneCust (Luxembourg). A site-directed mutagenesis experiment using two complementary mutagenic primers was performed for obtaining the catalytic mutant TvGSTX3^{C56S}. These genes were cloned into the recombinant plasmid pET26b in order to add a His-tag at the C-term for facilitating their purification (Table S1). Production step was made at 37 °C by using a heterologous system with *E. coli* Rosetta2™ (DE3) pLysS strain (Novagen) in a Luria Bertani Broth medium. The recombinant proteins were purified and eluted by using a column containing a Ni^{2+}-nitriloacetate-agarose resin, as described previously [22]. In addition, the expected molecular masses of the purified proteins were checked by mass spectrometry (electrospray ionization, for more details see the legend of Table S2).

Enzymatic measurements

The reductase activity of the studied TvGSTXs was tested against glutathionyl-phenylacetophenone (GS-PAP) and

GS-MEN, the substrates being synthetized as described previously [23]. The appearance of the expected products (phenylacetophenone and menadione) was followed by reverse phase chromatography. The assays were carried out as developed previously [7] and the concentration ranges were 5–200 μM and 500–2500 μM for GS-PAP and GS-MEN, respectively. Catalytic parameters were determined using varying substrate concentrations at saturating GSH concentration (4 mM) by fitting the Michaelis–Menten equation to the data using GraphPad Prism 5 software (GraphPad Software, La Jolla, CA, USA) (nonlinear regression).

The GST activity of the recombinant proteins toward 1-chloro 2,4-dinitrobenzene (CDNB) was also investigated by using a spectrophotometric method described previously [24].

Crystallization, X-ray data collection, processing, and refinement

Crystallization of TvGSTXs was conducted with the microbatch under oil method at 278 K. TvGSTX1 was crystallized by mixing 1 μL of protein (24 $mg{\cdot}mL^{-1}$) with 1 μL of solution consisting in 16% (w/v) polyethylene glycol 4000, 0.1 M pH 8.5 Tris-HCl buffer and 0.2 M magnesium chloride. TvGSTX3 wild-type was crystallized by mixing 2 μL of protein (7.5 $mg{\cdot}mL^{-1}$) with 1 μL of solution consisting in 20% (w/v) polyethylene glycol 8000, 0.1 M pH 6.5 sodium cacodylate buffer, and 0.2 M magnesium acetate. TvGSTX3-GSH crystals were obtained by cocrystallization using the same conditions for the native protein and 10 mM GSH. Monocrystals of $TvGSTX3^{C56S}$ were obtained under the same conditions as those for the wild-type protein plus 0.2 μL of 30% dextran sulfate sodium salt. All crystals were cryoprotected by a quick soaking in their mother liquor plus 20% glycerol. X-ray diffraction experiments were carried out on the ESRF beamline FIP BM30A (Grenoble, France). Data sets were indexed and integrated using XDS [25] and scaled with XSCALE or Aimless of the CCP4 suite [26]. The structure of TvGSTX3 was solved by molecular replacement with MOLREP [27] using coordinates of PcGSTX1 (Protein Data Bank code 3PPU) [8] as the search model. Structures were refined with PHENIX [28] and manually built with COOT [29]. All structures were validated with MOLPROBITY [30]. All figures were prepared by using Pymol (The PyMOL Molecular Graphics System, Version 2.0 Schrödinger, LLC).

Docking study

Molecular docking calculations of GS-PAP in TvGSTX3 were performed by using GOLD software (CCDC, Cambridge, UK) [31]. GS-PAP binding site was defined by specifying the sulfur atom of catalytic cysteine C56 (TvGSTX3 numbering) as the center of the cavity. Distance constraints were applied in order to (a) maintain the GSH moiety in its binding site (G site) and (b) to keep plausible stereochemistry of the phenylacetophenone moiety, as defined from crystal structures of similar molecules from the Cambridge Structural Database [32]. All other parameters were kept at their default values.

Phylogenetic analysis

GST Xi sequences were retrieved from the JGI database (https://jgi.doe.gov/) by the Protein Blast method using the sequences of TvGSTX1 and TvGSTX3 as templates. Putative GTSX sequences were curated manually. All sequences were aligned using the MAFFT multiple sequence alignment algorithm [33]. Phylogenetic analysis was performed using the neighbor-Joining method implemented in the MEGA7: Molecular Evolutionary Genetics Analysis Version 7.0 for bigger datasets [34].

Results and Discussion

TvGSTX1 reduces GS-MEN while TvGSTX3 reduces both GS-MEN and GS-PAP

Trametes versicolor possesses three GSTX-coding genes and the corresponding proteins are named TvGSTX1, TvGSTX2, and TvGSTX3. We purified recombinant TvGSTX1 and TvGSTX3, which shared 76% sequence identity (82% between TvGSTX1 and TvGSTX2, and 73% between TvGSTX2 and TvGSTX3). Mass spectrometry experiments conducted with the two His-tagged proteins revealed masses of 37 129 and 36 982 Da (Table S2) respectively, consistent with native proteins in their reduced state (devoid of any covalent adduct, e.g., Cys-S-SG). TvGSTXs were both tested with different substrates to assess their reductase activity (classic GSTX substrate GS-MEN; classic GSTO substrate GS-PAP), and GSH-transferase activity (classic GST substrate CDNB) (Table 1; Fig. S1).

Expectedly, no GSH-transferase activity was detected for any isoform, which is a typical trait for most Cys-GSTs [8,20]. TvGSTX1 and TvGSTX3 both have glutathionyl-hydroquinone reductase activity with the substrate GS-MEN (k_{cat}/K_m around 2200 $mM^{-1}{\cdot}min^{-1}$) in accordance with data obtained on GSTXs from various organisms (PcGSTX1 from *P. chrysosporium*, 600 $mM^{-1}{\cdot}min^{-1}$; PtGHR1 from poplar, 1000 $mM^{-1}{\cdot}min^{-1}$; YqjG from *E. coli*, 1100 $mM^{-1}{\cdot}min^{-1}$, Table 2). To complete the enzymatic profile of each isoform, the substrate GS-PAP (usually reduced by GSTOs but not GSTXs [17,20])

Table 1. Kinetic parameters of wild-type and mutant TvGSTXs. Data are represented as mean ± SD (n = 3). ND, not detected.

	GS-MEN	GS-PAP
	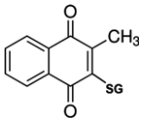	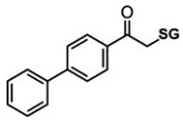
K_m (μM)		
TvGSTX1	921 ± 200	ND
TvGSTX3	2509 ± 257	207 ± 45
TvGSTX3 C56S	ND	ND
TvGSTX3 S295H	1055 ± 189	4861 ± 1576
k_{cat} (min^{-1})		
TvGSTX1	1966 ± 201	ND
TvGSTX3	5619 ± 361	1895 ± 257
TvGSTX3 C56S	ND	ND
TvGSTX3 S295H	205 ± 16	99 ± 26
k_{cat}/K_m ($mM^{-1}·min^{-1}$)		
TvGSTX1	2196 ± 198	ND
TvGSTX3	2240 ± 143	9152 ± 1236
TvGSTX3 C56S	ND	ND
TvGSTX3 S295H	195 ± 15	15 ± 5

was tested. While TvGSTX1 behaves like previously studied GSTXs and is inactive with GS-PAP, TvGSTX3 surprisingly reduces this substrate with a catalytic efficiency of 9152 $mM^{-1}·min^{-1}$, below but comparable to PcGSTOs (Table 2).

In order to further characterize the peculiar isoform TvGSTX3, we studied the mutant in which a serine residue replaced the catalytic cysteine C56 ($TvGSTX3^{C56S}$). As expected, $TvGSTX3^{C56S}$ no longer reduced GS- derivatives consistently with data obtained with $PcGSTX1^{C86S}$ in a previous study [8]. However, $TvGSTX3^{C56S}$ acquired GSH-transferase activity with CDNB (Fig. S1). The same property was observed for $PcGSTO4^{C37S}$ [20] but not for $PcGSTX1^{C86S}$ [8]. As a conclusion to these experiments, TvGSTX3 isoform has the singular catalytic property to behave both like a GHR and a GSTO. It prompted us to determine its crystal structure.

TvGSTX1 and TvGSTX3 share similar structures with differences in the active sites

A crystallographic study was undertaken on TvGSTX1 and TvGSTX3. We solved four structures: wild-type $TvGSTX1^{WT}$, wild-type $TvGSTX3^{WT}$, wild-type $TvGSTX3^{GSH}$ cocrystallized with GSH, and $TvGSTX3^{C56S}$ mutant bound with dextran sulfate used as a crystallization additive (Table S3). The three structures that correspond to isoform TvGSTX3 are almost identical (largest rmsd of 0.267 Å for 508 Cα aligned between $TvGSTX3^{WT}$ and $TvGSTX3^{C56S}$, Table S4). The only difference lies in the N-terminal end visible in electron density starting from Asp21 (monomer A) in $TvGSTX3^{WT}$ and from Ala28 (monomers A) in $TvGSTX3^{GSH}$ and $TvGSTX3^{C56S}$. This suggests some flexibility upon ligand binding. Superimposed structures of $TvGSTX1^{WT}$ and $TvGSTX3^{WT}$ indicate a high degree of likeness (rmsd of 0.569 Å for 488 Cα). Both isoforms display their highest structural homology with PcGSTX1 (rmsd of 0.546 Å for 563 Cα and sequence identity of 70% between TvGSTX1 and PcGSTX1) (Fig. 2). In brief, TvGSTX monomers adopt the GST fold (N-terminal domain β1α1β2α2β3β4α3, and C-terminal domain α4α5α6α7α8α9) with the specific features of the Xi class, which include a long insertion loop between β2-α2, extended N- and C-terminal coils, and an atypical dimerization mode by the helical domains [8].

Table 2. Reductase activities of characterized GSTXs and GSTOs toward GS-hydroquinones or GS-acetophenones. ND means that reductase activity was not detected. For all GSTXs, glutathionyl-hydroquinone reductase activity was assessed by using GS-MEN substrate. For all GSTOs, glutathionyl-acetophenone reductase activity was assessed by using GS-PAP substrate [20], except for HsGSTO isoforms for which GS-nitroacetophenone was used [9].

			Catalytic efficiency (k_{cat}/K_m, $mM^{-1}·min^{-1}$)		
Class	Organism	Enzyme	GS-hydroquinone	GS-acetophenone	References
GSTX	*Escherichia coli*	EcYqjG	1100	ND	Xun (2010) [18]; Green (2012) [14]
	Saccharomyces cerevisiae	ScECM4	812	ND	Schwartz (2016) [15]
	Phanerochaete chrysosporium	PcGSTX1	600	ND	Meux (2011) [8]
		TvGSTX1	2196	ND	This study
	Trametes versicolor	TvGSTX3	2240	9152	This study
		$TvGSTX3^{S295H}$	195	15	This study
GSTO	*Phanerochaete chrysosporium*	PcGSTO3	ND	2427	Meux (2011) [8]
		PcGSTO4	ND	52 173	Meux (2013) [20]
	Homo sapiens	HsGSTO1-1	ND	780	Board (2007) [9]; Xun (2010) [18]
		HsGSTO2-2	ND	ND	Board (2007) [9]; Xun (2010) [18]

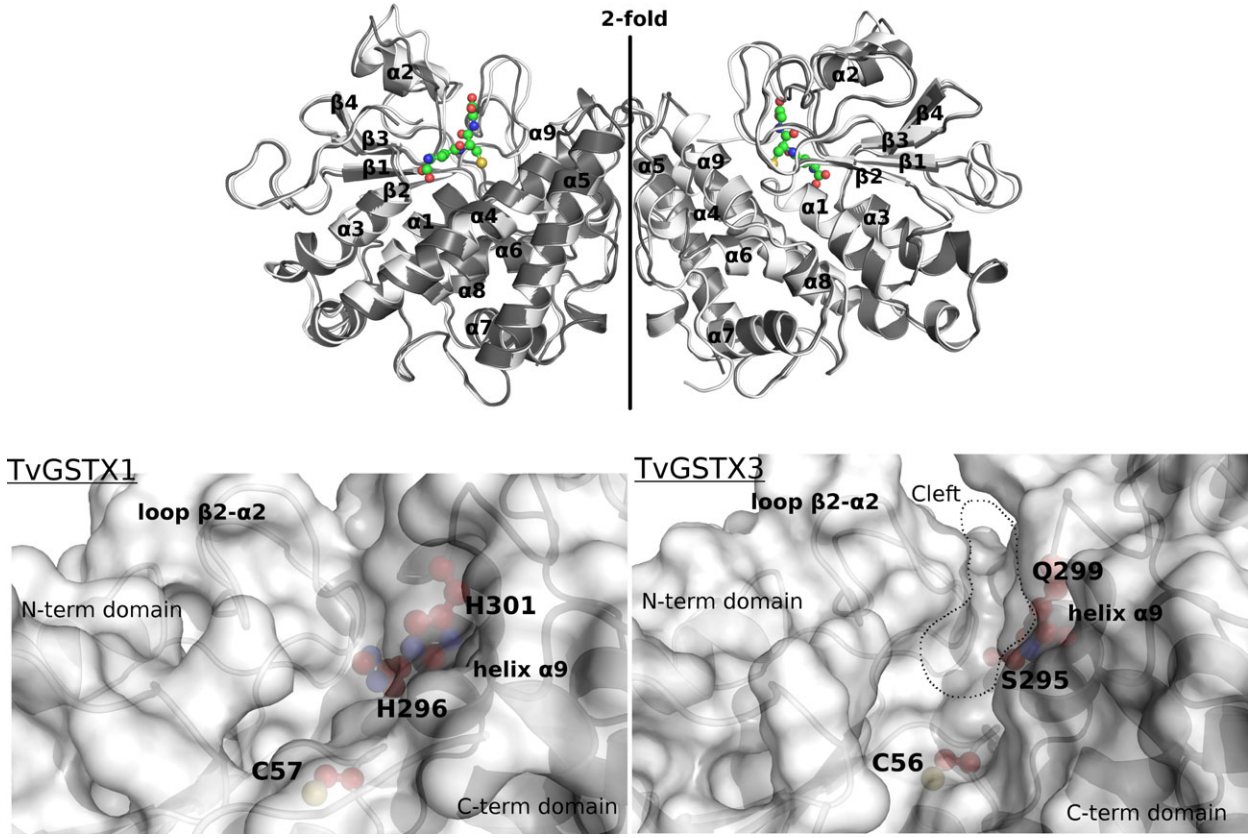

Fig. 2. Crystal structures of TvGSTX1 and TvGSTX3. Top panel: Superimposition of TvGSTX1 dimer (white) and TvGSTX3 dimer (black) complexed with GSH. Secondary structure elements are labeled and GSH is represented as green sticks and spheres. Bottom panels: Active sites of TvGSTX1 (left) and TvGSTX3 (right). Differences present in TvGSTX3 helix α9 create an accessible cleft (circled by a dotted line) near the catalytic cysteine C56. Molecular surfaces are represented in white transparency. Side chains are displayed as red sticks and spheres.

A detailed structural comparison of the active sites was done in an attempt to explain the catalytic profile of TvGSTX3 with respect to the X1 isoform. Both crystallographic structures indicate active sites that share many features in common. The determination of TvGSTX3^{GSH} structure enabled the identification of residues essential for glutathione recognition (G site) (Fig. S2). GSH interacts mainly through polar contacts with the side chain or the main chain of the residues W89, R125, V128, E143, and S144. This binding site is strictly conserved in TvGSTX1, as in GSTX structures determined so far (Fig. S3). The Cys-GSTs and the tyrosine triad are arranged in the same way in both isoforms. Significant differences are observed at the H site. On one hand, the residues that line the putative quinone-binding site (H site) of TvGSTX1 are identical to those suggested from the structures of PcGSTX1[8], ScECM4[15], and EcYqjG [14]. They include residues W58 from helix α1, Y194 and F198 from α4, H296, and H301 from helix α9. On the other hand, both histidine residues are not conserved in TvGSTX3 and helix α9 is one residue shorter at its C-terminal end (Fig. 2). Indeed, the ^{295}SYYA-Q^{299} sequence in TvGSTX3 replaces the ^{296}HYYWSH^{301} sequence of TvGSTX1. These differences create an additional solvent accessible cleft in the active site of TvGSTX3, which is located between helix α9 and loop β2-α2. Its presence is mainly due to the replacement of the first histidine (H296 in TvGSTX1) by the smaller S295. The next section discusses the potential of this cleft as a binding site for the phenylacetophenone moiety of the TvGSTX3 substrate GS-PAP.

In TvGSTX3^{C56S} crystal structure, inspection of electron density maps revealed the presence of a crystallization additive bound to the active site (Fig. S4). This ligand was identified as three units of dextran sulfate (sulfated glycosidic polymer with α-1,6 bonds). Dextran sulfate fully occupies both G and H sites. Sidechains of residues F197, S295, and N301 move to accommodate the ligand that is stabilized mainly by its

sulfate groups. Five hydrogen bonds are established between the dextran and side chains from R112 (α2), R125 (α2-β3, involved in GSH binding), Y193 (α4, which belongs to the tyrosine cluster), Q299 (α9), and N301 (C-terminal tail). The presence of a polysaccharide in the active site may be of biological relevance. Indeed, it was shown that GSTX ScECM4 would be involved in the biosynthesis of the fungal cell wall [35], which is mainly constituted by carbohydrate polymers (chitin, β-1,3- and β-1,6- glucans)[36].

TvGSTX3 has a new cleft suited for GS-PAP binding

Enzymatic assays showed that TvGSTX1 and TvGSTX3 reduced GS-MEN as expected and unveiled an additional activity for TvGSTX3 in reducing GS-PAP. Crystallographic study revealed an additional accessible cleft in the active site of TvGSTX3 when compared to TvGSTX1 and known GSTX structures. A less bulky serine residue in helix α9 of TvGSTX3 (S295) partly explains the presence of the new cleft. A histidine residue occupies this position in TvGSTX1 (H296). We generated the mutation S295H to evaluate the importance of this position in the catalytic diversity of TvGSTX3. The catalytic efficiency of $TvGSTX3^{S295H}$ with GS-PAP dropped to 15 $mM^{-1}{\cdot}min^{-1}$ (resulting in a 623-fold loss with respect to the wild-type protein) by decreasing both the apparent affinity for GS-PAP (K_m value multiplied by 24) and the turnover number (k_{cat} value divided by 19, Table 1). The GS-MEN activity did not show such a change. $TvGSTX3^{S295H}$ was still active with GS-MEN though with a 10-fold drop in k_{cat}/K_m caused by a decrease of the catalytic rate only. This suggests that the histidine side chain does not cause a decrease in the ability to bind GS-MEN, but that the conformation of the bound substrate is not ideal with respect to the catalytic mechanism. Our results show that a single mutation in TvGSTX3 helix α9 leads to the near loss of the GSTO activity while retaining the GSTX activity.

We performed a molecular docking study to evaluate if the new cleft in the active site of TvGSTX3 and its activity against GS-PAP could be related. We assumed that the glutathionyl moiety of GS-PAP would bind to the G site in a conformation similar to reduced GSH in $TvGSTX3^{GSH}$ and we applied atomic position constraints accordingly during molecular docking. Additionally, distance constraints based on small molecule crystal structures were also applied to the phenyl-acetophenone group to maintain plausible stereochemistry. The constrained docking suggests three regions in the active site, which could be competent for phenylacetophenone moiety binding (Fig. 3). Indeed, we found a mean distance between the sulfur atom of the catalytic cysteine (C56) and the thioether sulfur atom of GS-PAP near 4 Å. The first region corresponds to the new cleft described in the previous section, between helix α9 and the adjacent loop β2-α2. The side chains of Phe84, Tyr193, Ser295, Ala298, and Gln299 ensure a hydrophobic environment and a snug fit for the phenylacetophenone moiety. These residues interact with the ligand dextran sulfate in the $TvGSTX3^{C56S}$ crystal structure (see above). The second region is located along helices α4 and α9 with Phe197 and Gln299 as the residues potentially engaged in stabilization of the GSH adduct. The last region is perpendicular to the helix α4 with the side chains of Trp58, Asn190, and Tyr193 as the closest neighbors of the phenylacetophenone moiety. This third region corresponds to the menadione moiety binding site in the crystal structure of EcYqjG in complex with GS-MEN [14]. Taken together, the mutagenesis study and the docking simulation support the reduction of GS-PAP with its phenylacetophenone-moiety bound in the cleft present in TvGSTX3 but not in TvGSTX1. In the next section, we investigate the differences between these two isoforms from a phylogenetic point of view.

Helix α9 is prone to mutations in the active site of fungal GSTXs

Putative GSTX sequences were retrieved from the 49 fungal genomes that were used in two previous evolutionary studies [37,38]. TvGSTX1 and TvGSTX3 were

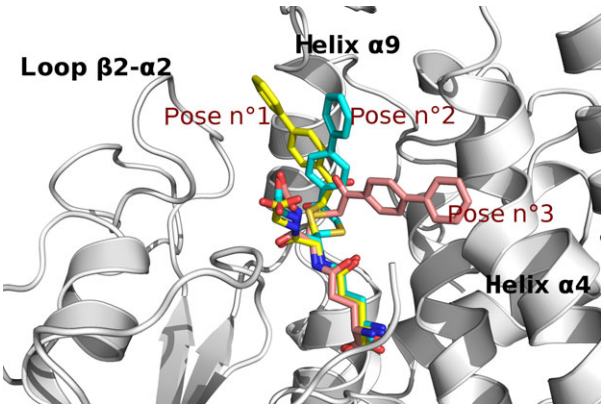

Fig. 3. Docking poses of GS-PAP in TvGSTX3 active site. Representative binding poses (*n* °1 in yellow, *n* °2 in cyan and *n* °3 in salmon) of GS-PAP were predicted by GOLD in TvGSTX3 active site. Region of pose *n* °1 is located in the cleft between loop β2-α2 and helix α9.

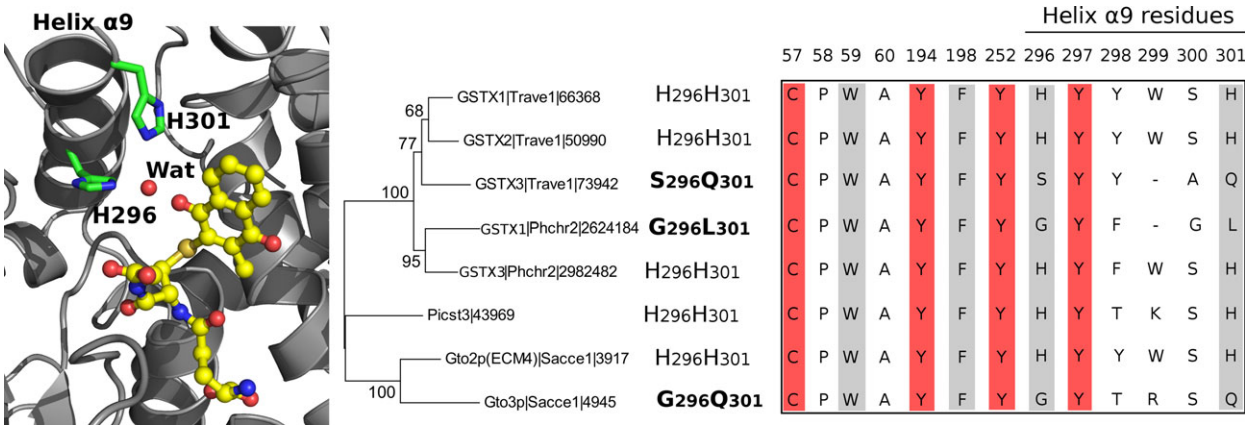

Fig. 4. Neighbor-joining analysis of fungal GSTX revealed variations at helix α9. GS-MEN in TvGSTX1 active site (model based on the superimposition with YqjG complexed with GS-MEN) is shown in left panel. The histidine pair (side chains in green sticks) that coordinates a water molecule in the vicinity of GS-MEN (yellow sticks) is labeled. Neighbor-Joining analysis of representative GSTX sequences is displayed in the middle panel. Sequences for which the histidine pair is absent are in bold and original residues are indicated. Bootstrap values are indicated at nodes. Trave: *Trametes versicolor*, Phchr: *Phanerochaete chrysosporium*, Picst: *Pichia stipitis*, Sacce: *Saccharomyces cerevisiae*. GSTX important residues are indicated in the right panel : catalytic residues are colored red, putative (hydro) quinone-binding site residues are colored gray. Numbering is based on TvGSTX1 sequence.

used as the queries for Protein BLAST searches. This set of sequences was aligned and used to perform a phylogenetic study (Fig. S5). The results suggest the presence of at least one GSTX isoform in each organism. Larger numbers of GSTX isoforms (up to five in *Oidiodendron maius*) are found in two groups of organisms: ascomycetes and saprotrophic basidiomycetes (three isoforms in *T. versicolor*). Extensions of the GST classes Ure2p and GSTFuAs have been previously reported in wood decayers, with more than 10 isoforms for some of them [39,40]. In these classes, the sequences cluster in an organism-specific manner, which could reflect a recent diversification [40,41]. We observed a similar trend for GSTXs.

The aligned sequences reveal the invariance of the catalytic cysteine as well as of the three tyrosine residues that form the catalytic triad (Fig. S3). Most residues that constitute the substrate-binding sites (G and H sites) are also well conserved. Interestingly, variations are found at C-terminal helix α9, which is a part of the H site bottom (Fig. 4). Position 296 (TvGSTX1 numbering) is occupied by a His residue in 61% of the sequences or by a smaller residue in 28% (a Gly residue in most cases, S295 in TvGSTX3). This residue is critical in providing a large cleft in TvGSTX3 potentially related to its catalytic diversity. An additional difference is found at position 301 with a histidine residue in 55% of the sequences (H301 in TvGSTX1 and Q299 in TvGSTX3). The sequences show that residues at positions 296 and 301 (TvGSTX1 numbering) tend to coevolve. Indeed, when the first position is occupied by a non-His residue, so does the second one (81% of the cases). Thus, the helix α9 region is probably prone to mutations as previously reported for solvent-exposed helices [42,43]. This variable region could promote catalytic diversity in the GSTX family, as shown for TvGSTX3 isoform.

Conclusion

In this study, we show that GSTX1 and GSTX3 from *T. versicolor* have the usual GS-(hydro)quinone reductase activity while TvGSTX3 has an additional glutathionyl-acetophenone reductase activity, a feature of GSTOs. Both have the GSTX fold and exhibit structural differences in the active site located at the C-terminal end of helix α9. In TvGSTX3, the presence of smaller residues creates a new cleft that could offer favorable environment for GS-PAP and could explain the substrate diversity observed for this isoform, in accordance with mutagenesis and docking experiments. This peculiar H site makes TvGSTX3 a dual Cys-GST, which shares the substrate specificities of Xi and Omega classes. An examination of fungal GSTX sequences shows that the case of TvGSTX3 should not be unique. This suggests additional functions of GSTXs with respect to their initially assigned GHR activity. Further studies are necessary to clarify whether isoforms from different organisms also exhibit substrate diversity.

Acknowledgements

The authors would like to thank ESRF for beamtime, and the staff of beamline BM30A for data collections. The authors appreciated the access to the 'Plateforme de mesures de diffraction X' of the University of Lorraine with crystal testing.

Funding

This work has been funded by the Laboratory of Excellence Advanced Research on the Biology of Tree and Forest Ecosystems (ARBRE grant ANR 11 LABX 0002 01). The authors acknowledge financial support from the 'Impact Biomolecules' project of the 'Lorraine Université d'Excellence' (Investissements d'avenir – ANR).

Author contributions

CD, FF, EG, and MMR conceived and supervised the study. CD, EG, MS, and TP designed experiments. MS, TP, AD, GM, and CD performed experiments. MS, TR, TP, CD, GM, EG, and MMR analyzed data. MS, FF, and CD wrote the manuscript. All authors made manuscript revisions.

Data accessibility

Coordinates and structures factors of $TvGSTX1^{WT}$, $TvGSTX3^{WT}$, $TvGSTX3^{GSH}$ and $TvGSTX3^{C56S}$ have been deposited in the Protein Data Bank under accession codes 6GC9, 6GCA, 6GCB and, 6GCC, respectively.

References

1 Lallement PA, Brouwer B, Keech O, Hecker A and Rouhier N (2014) The still mysterious roles of cysteine-containing glutathione transferases in plants. *Front Pharmacol* **5**, 192.

2 Rossjohn J, Polekhina G, Feil SC, Allocati N, Masulli M, Ilio CD and Parker MW (1998) A mixed disulfide bond in bacterial glutathione transferase: functional and evolutionary implications. *Structure* **6**, 721–734.

3 Cromer BA, Morton CJ, Board PG and Parker MW (2002) From glutathione transferase to pore in a CLIC. *Eur Biophys J* **31**, 356–364.

4 Lallement PA, Roret T, Tsan P, Gualberto JM, Girardet JM, Didierjean C, Rouhier N and Hecker A (2016) Insights into ascorbate regeneration in plants: investigating the redox and structural properties of dehydroascorbate reductases from Populus trichocarpa. *Biochem J* **473**, 717–731.

5 Board PG, Coggan M, Chelvanayagam G, Easteal S, Jermiin LS, Schulte GK, Danley DE, Hoth LR, Griffor MC, Kamath AV *et al.* (2000) Identification, characterization, and crystal structure of the Omega class glutathione transferases. *J Biol Chem* **275**, 24798–24806.

6 Dixon DP and Edwards R (2010) Roles for stress-inducible lambda glutathione transferases in flavonoid metabolism in plants as identified by ligand fishing. *J Biol Chem* **285**, 36322–36329.

7 Lallement PA, Meux E, Gualberto JM, Prosper P, Didierjean C, Saul F, Haouz A, Rouhier N and Hecker A (2014) Structural and enzymatic insights into Lambda glutathione transferases from Populus trichocarpa, monomeric enzymes constituting an early divergent class specific to terrestrial plants. *Biochem J* **462**, 39–52.

8 Meux E, Prosper P, Ngadin A, Didierjean C, Morel M, Dumarçay S, Lamant T, Jacquot JP, Favier F and Gelhaye E (2011) Glutathione transferases of Phanerochaete chrysosporium: S-glutathionyl-p-hydroquinone reductase belongs to a new structural class. *J Biol Chem* **286**, 9162–9173.

9 Board PG and Anders MW (2007) Glutathione transferase omega 1 catalyzes the reduction of S-(phenacyl)glutathiones to acetophenones. *Chem Res Toxicol* **20**, 149–154.

10 Morel M, Meux E, Mathieu Y, Thuillier A, Chibani K, Harvengt L, Jacquot JP and Gelhaye E (2013) Xenomic networks variability and adaptation traits in wood decaying fungi. *Microb Biotechnol* **6**, 248–263.

11 Brock J, Board PG and Oakley AJ (2013) Structural insights into omega-class glutathione transferases: a snapshot of enzyme reduction and identification of a non-catalytic ligandin site. *PLoS ONE* **8**, e60324.

12 Mashiyama ST, Malabanan MM, Akiva E, Bhosle R, Branch MC, Hillerich B, Jagessar K, Kim J, Patskovsky Y, Seidel RD *et al.* (2014) Large-scale determination of sequence, structure, and function relationships in cytosolic glutathione transferases across the biosphere. *PLoS Biol* **12**, e1001843.

13 Huang Y, Xun R, Chen G and Xun L (2008) Maintenance role of a glutathionyl-hydroquinone lyase (PcpF) in pentachlorophenol degradation by Sphingobium chlorophenolicum ATCC 39723. *J Bacteriol* **190**, 7595–7600.

14 Green AR, Hayes RP, Xun L and Kang C (2012) Structural understanding of the glutathione-dependent reduction mechanism of glutathionyl-hydroquinone reductases. *J Biol Chem* **287**, 35838–35848.

15 Schwartz M, Didierjean C, Hecker A, Girardet JM, Morel-Rouhier M, Gelhaye E and Favier F (2016) Crystal structure of saccharomyces cerevisiae ECM4, a Xi-class glutathione transferase that reacts with glutathionyl-(hydro)quinones. *PLoS ONE* **11**, e0164678.

16 Garcera A, Barreto L, Piedrafita L, Tamarit J and Herrero E (2006) Saccharomyces cerevisiae cells have three Omega class glutathione S-transferases acting as 1-Cys thiol transferases. *Biochem J* **398**, 187–196.
17 Lallement PA, Meux E, Gualberto JM, Dumarcay S, Favier F, Didierjean C, Saul F, Haouz A, Morel-Rouhier M, Gelhaye E *et al*. (2015) Glutathionyl-hydroquinone reductases from poplar are plastidial proteins that deglutathionylate both reduced and oxidized glutathionylated quinones. *FEBS Lett* **589**, 37–44.
18 Xun L, Belchik SM, Xun R, Huang Y, Zhou H, Sanchez E, Kang C and Board PG (2010) S-Glutathionyl-(chloro) hydroquinone reductases: a novel class of glutathione transferases. *Biochem J* **428**, 419–427.
19 Lam LK, Zhang Z, Board PG and Xun L (2012) Reduction of benzoquinones to hydroquinones *via* spontaneous reaction with glutathione and enzymatic reaction by S-glutathionyl-hydroquinone reductases. *Biochemistry* **51**, 5014–5021.
20 Meux E, Morel M, Lamant T, Gerardin P, Jacquot JP, Dumarcay S and Gelhaye E (2013) New substrates and activity of Phanerochaete chrysosporium Omega glutathione transferases. *Biochimie* **95**, 336–346.
21 Belchik SM and Xun L (2011) S-glutathionyl-(chloro) hydroquinone reductases: a new class of glutathione transferases functioning as oxidoreductases. *Drug Metab Rev* **43**, 307–316.
22 Deroy A, Saiag F, Kebbi-Benkeder Z, Touahri N, Hecker A, Morel-Rouhier M, Colin F, Dumarcay S, Gérardin P, Gelhaye E *et al*. (2015) The GSTome reflects the chemical environment of white-rot fungi. *PLoS ONE* **10**, e0137083.
23 Nickerson WJ, Falcone G and Strauss G (1963) Studies on quinone-thioethers. I. mechanism of formation and properties of thiodione*. *Biochemistry* **2**, 537–543.
24 Habig WH, Pabst MJ and Jakoby WB (1974) Glutathione S-transferases. The first enzymatic step in mercapturic acid formation. *J Biol Chem* **249**, 7130–7139.
25 Kabsch W (2010) XDS. *Acta Crystallogr D Biol Crystallogr* **66**, 125–132.
26 Winn MD, Ballard CC, Cowtan KD, Dodson EJ, Emsley P, Evans PR, Keegan RM, Krissinel EB, Leslie AG, McCoy A *et al*. (2011) Overview of the CCP4 suite and current developments. *Acta Crystallogr D Biol Crystallogr* **67**, 235–242.
27 Vagin A and Teplyakov A (2010) Molecular replacement with MOLREP. *Acta Crystallogr D Biol Crystallogr* **66**, 22–25.
28 Adams PD, Afonine PV, Bunkóczi G, Chen VB, Davis IW, Echols N, Headd JJ, Hung LW, Kapral GJ, Grosse-Kunstleve RW *et al*. (2010) PHENIX: a comprehensive Python-based system for macromolecular structure solution. *Acta Crystallogr D Biol Crystallogr* **66**, 213–221.
29 Emsley P and Cowtan K (2004) Coot: model-building tools for molecular graphics. *Acta Crystallogr D Biol Crystallogr* **60**, 2126–2132.
30 Davis IW, Murray LW, Richardson JS and Richardson DC (2004) MOLPROBITY: structure validation and all-atom contact analysis for nucleic acids and their complexes. *Nucleic Acids Res* **32**, W615–W619.
31 Verdonk ML, Cole JC, Hartshorn MJ, Murray CW and Taylor RD (2003) Improved protein–ligand docking using GOLD.. *Proteins* **52**, 609–623.
32 Groom CR, Bruno IJ, Lightfoot MP and Ward SC (2016) The Cambridge structural database. *Acta Crystallogr B Struct Sci Cryst Eng Mater* **72**, 171–179.
33 Katoh K and Standley DM (2013) MAFFT multiple sequence alignment software version 7: improvements in performance and usability. *Mol Biol Evol* **30**, 772–780.
34 Kumar S, Stecher G and Tamura K (2016) MEGA7: molecular evolutionary genetics analysis version 7.0 for Bigger Datasets. *Mol Biol Evol* **33**, 1870–1874. https://doi.org/10.1093/molbev/msw054
35 Lussier M, White AM, Sheraton J, di Paolo T, Treadwell J, Southard SB, Horenstein CI, Chen-Weiner J, Ram AF, Kapteyn JC *et al*. (1997) Large scale identification of genes involved in cell surface biosynthesis and architecture in Saccharomyces cerevisiae. *Genetics* **147**, 435–450.
36 Osumi M (1998) The ultrastructure of yeast: Cell wall structure and formation. *Micron* **29**, 207–233.
37 Floudas D, Binder M, Riley R, Barry K, Blanchette RA, Henrissat B, Martínez AT, Otillar R, Spatafora JW, Yadav JS *et al*. (2012) The Paleozoic origin of enzymatic lignin decomposition reconstructed from 31 fungal genomes. *Science* **336**, 1715–1719.
38 Kohler A, Kuo A, Nagy LG, Morin E, Barry KW, Buscot F, Canbäck B, Choi C, Cichocki N, Clum A *et al*. (2015) Convergent losses of decay mechanisms and rapid turnover of symbiosis genes in mycorrhizal mutualists. *Nat Genet* **47**, 410–415.
39 Morel M, Ngadin AA, Droux M, Jacquot JP and Gelhaye E (2009) The fungal glutathione S-transferase system. Evidence of new classes in the wood-degrading basidiomycete Phanerochaete chrysosporium. *Cell Mol Life Sci* **66**, 3711–3725.
40 Mathieu Y, Prosper P, Favier F, Harvengt L, Didierjean C, Jacquot JP, Morel-Rouhier M and Gelhaye E (2013) Diversification of fungal specific class a glutathione transferases in saprotrophic fungi. *PLoS ONE* **8**, e80298.
41 Roret T, Thuillier A, Favier F, Gelhaye E, Didierjean C and Morel-Rouhier M (2015) Evolutionary divergence of Ure2pA glutathione transferases in wood degrading fungi. *Fungal Genet Biol* **83**, 103–112.
42 Goldman N, Thorne JL and Jones DT (1998) Assessing the impact of secondary structure and solvent

accessibility on protein evolution. *Genetics* **149**, 445–458.

43 Abrusan G and Marsh JA (2016) Alpha helices are more robust to mutations than beta strands. *PLoS Comput Biol* **12**, e1005242.

Supporting information

Additional supporting information may be found online in the Supporting Information section at the end of the article.

Table S1. Nucleotide sequences of TvGSTX1^{WT} and TvGSTX3 $^{WT,\ C56S\ and\ S295H}$ designed to contain a His-tag at the end of the C-terminal part.

Table S2. Mass spectrometry analysis of recombinant TvGSTXs.

Table S3. Diffraction and refinement statistics.

Table S4. Superimpositions of the TvGSTX structures.

Fig. S1. Glutathione transferase activity toward CDNB for the mutant TvGSTX3^{C56S}.

Fig. S2. Glutathione bound to TvGSTX3 G site.

Fig. S3. Multiple sequence alignment of putative fungal GSTX.

Fig. S4. Dextran sulfate complexed in TvGSTX3 C56S active site.

Fig. S5. Neighbor-Joining analysis of putative GSTX sequences from various fungi.